Charge carrier trapping processes in lanthanide doped La-, Gd-, Y-, and LuPO4

Lyu, Tianshuai; Dorenbos, Pieter

DOI
10.1039/C7TC05221A

Publication date
2017

Document Version
Accepted author manuscript

Published in
Journal of Materials Chemistry C: materials for optical and electronic devices

Journal of Materials Chemistry C

Accepted Manuscript

ROYAL SOCIETY OF CHEMISTRY

rsc.li/materials-c

View Article Online
DOI: 10.1039/C7TC05221A

Table of Contents Graphic

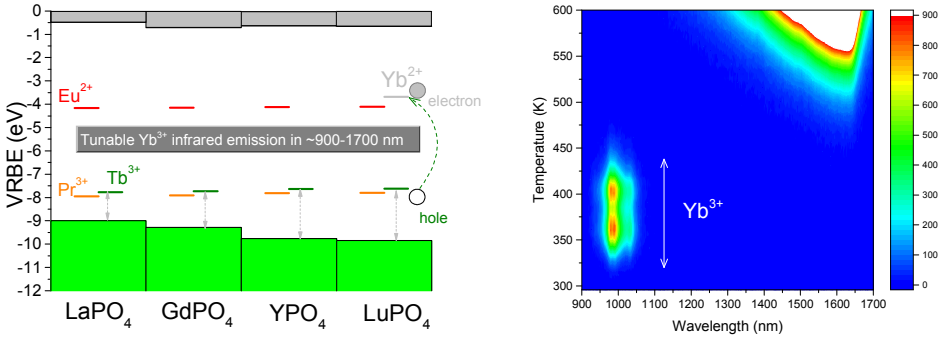

View Article Online
DOI: 10.1039/C7TC05221A

Charge carrier trapping processes in lanthanide doped La-, Gd-, Y-, and $LuPO_4$

Tianshuai Lyu* and Pieter Dorenbos

Delft University of Technology, Faculty of Applied Sciences, Department of Radiation Science and Technology, section Luminescence Materials, Mekelweg 15, 2629JB Delft, The Netherlands
E-mail: T.lyu-1@tudelft.nl

Abstract

Various methods for deliberate design electron and hole trapping materials are explored with a study on double lanthanide doped rare earth ortho phosphates. Cerium acts as recombination center while lanthanide codopants as electron trapping centers in $LaPO_4$:0.005Ce^{3+},0.005Ln^{3+}. The electron trap depth generated by lanthanide codopants can be tailored by the choice of lanthanide, and for fixed set of lanthanide dopants like in $Gd_{1-x}La_xPO_4$:0.005Ce^{3+},0.005Ho^{3+} solid solutions by changing x leading to conduction band (CB) engineering. Here, the electrons liberated from Ho^{2+} recombine through the conduction band at Ce^{4+} to yield Ce^{3+} 5d-4f emission. In contrast, samarium, europium and ytterbium are recombination centers, while Tb^{3+} and Pr^{3+} act as hole trapping centers in double lanthanide doped YPO_4. For Tb^{3+} and Pr^{3+} codopants recombination is realized via hole release rather than the more common reported electron release. The holes recombine via the valence band with the electrons trapped at Yb^{2+}, Sm^{2+}, or Eu^{2+} to generate 4f-4f luminescence from Yb^{3+}, Sm^{3+}, or Eu^{3+}. Lu^{3+} was introduced in YPO_4 to tailor the valence band (VB) energy and to tune the hole trap depths of Tb^{3+} and Pr^{3+} in $Y_{1-x}Lu_xPO_4$:0.005Ln^{3+} solid solutions. Our results promote the deliberate design electron and hole trapping materials from deep understanding of trap level locations and on the transport and trapping processes of charge carriers.

View Article Online
DOI: 10.1039/C7TC05221A

1. Introduction

The trapping and release processes of charge carriers are of interest for practical applications and from a theoretical point of view[1, 2]. When electron and hole trapping materials are exposed to high energy radiation, for instance, beta radiation or ultraviolet (UV) light, free electron and hole charge carriers will be generated and then trapped in trapping centers, which are usually lattice defects or impurities[3]. The trapped holes or electrons can be released by optical, thermal, or mechanical excitation, ultimately yielding photon emission at wavelengths that can range from ultraviolet to infrared, depending on the recombination centers and type of compound[1, 4]. For storage phosphors applied in X-ray imaging, deep traps (~2 eV) are needed to avoid thermal fading at room temperature (RT)[5]. Relatively shallow traps (<~0.7 eV) are required to generate RT afterglow[6, 7]. So, if we can control the trap depth of holes or electrons, then in principle one may engineer or deliberate design storage and afterglow properties.

The electron trapping and release process has been widely investigated[1, 8-11]. Ueda et al. reported the valence change of Ce^{3+} and Cr^{3+} in $Y_3Al_2Ga_3O_{12}$ persistent phosphors using X-ray absorption near edge structure (XANES) spectroscopy[12]. Concentration of both Ce^{4+} and Cr^{2+} rises after exposing the sample to UV light. This shows that Ce^{3+} is the electron donor and the electrons produced via photoionization can be trapped by Cr^{3+} electron trapping centers. By thermal excitation at room temperature, the electrons trapped at Cr^{2+} will be liberated slowly to the conduction band and then recombine with Ce^{4+} to finally generate Ce^{3+} emission peaked at ~510 nm[13]. A similar partial oxidation of Eu^{2+} to Eu^{3+} after UV light excitation is observed in the well-known persistent phosphor $SrAl_2O_4:Eu^{2+},Dy^{3+}$ using XANES[14].

Holes can also be liberated to recombine with a luminescence center. The hole transport can be as a migrating V_k center or through the valence band[2]. Such hole trapping and release processes are scarcely reported. One of the few cases is by Chakrabarti et al. in the 1980s who observed that cerium acts as a hole trapping center and samarium as a recombination center in $MgS:Ce^{3+},Sm^{3+}$ after UV light excitation[15]. The holes liberate from Ce^{4+} earlier than electrons from Sm^{2+} and recombine with Sm^{2+} generating Sm^{3+} 4f-4f emission. The other two examples are from studies by Luo et al. on $Gd_{1-x}La_xAlO_3$[7] and RE_2O_2S.[2] The trap depth of the Tb^{3+} hole trapping center in $Gd_{1-x}La_xAlO_3$ can be adjusted by changing x leading to valence band energy changes. In $RE_2O_2S:Ti^{4+}$ a hole release process leading to Ti^{4+} charge transfer emission was identified.

The rare reporting on hole trapping and release processes is associated with a lack in our knowledge on how to distinguish such a hole trapping process from an electron trapping process. For that we need information on where the hole or electron traps are located within the bandgap. It is not until 2012 that the chemical shift model was published that enables one to create a vacuum referred binding energy (VRBE) diagram. One may now compare the binding energy at the valence band top or conduction band bottom in various compounds with respect to a same reference energy[16-19]. This model shows that the VRBE in the $4f^n$ ground state of trivalent and divalent lanthanides is almost independent on the type of compound[20-23].

View Article Online
DOI: 10.1039/C7TC05221A

Consequently, lanthanide related hole trap depth can be tuned by altering the VRBE at the top of the valence band and electron trap depth through tailoring the VRBE at the bottom of the conduction band[7].

In this paper, based on the constructed VRBE diagrams and band gap engineering, we will show how to deliberate design storage phosphors through precisely controlling both the releases of electrons and of holes. La-, Gd-, Y-, and $LuPO_4$ phosphates were selected as hosts due to their simple structures with only one site to substitute for a trivalent lanthanide. To demonstrate the design concept, the constructed VRBE diagram of YPO_4 is already shown in Fig. 1. The zigzag curves I and II link the VRBE of an electron in the ground states of the divalent and trivalent lanthanides, respectively. Such diagram is very useful to decide what shallow and deep electron hole trap combinations can be used to arrive at specific properties. For example, Eu^{3+} 4f-4f emission will be observed for the Eu^{3+}-Tb^{3+} pair in YPO_4 after hole release from Tb^{4+} since it is predicted that Eu^{3+} will act as a much deeper electron trap than Tb^{3+} as a hole trap.

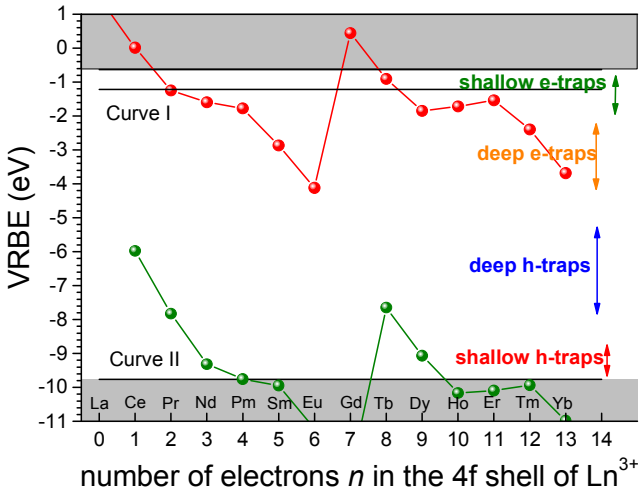

Fig. 1. Vacuum referred binding energy (VRBE) diagram of YPO_4 with various Ln traps.

Fig. 2 shows the stacked VRBE diagram for the four $REPO_4$ compounds studied in this work. It shows that the lanthanide trap depth can be engineered by changing the VRBE at the conduction band bottom or valence band top. For instance, the hole trap depth of Pr^{3+} or Tb^{3+} can be decreased by replacing Lu^{3+} by Y^{3+}, Gd^{3+}, or La^{3+}.

View Article Online
DOI: 10.1039/C7TC05221A

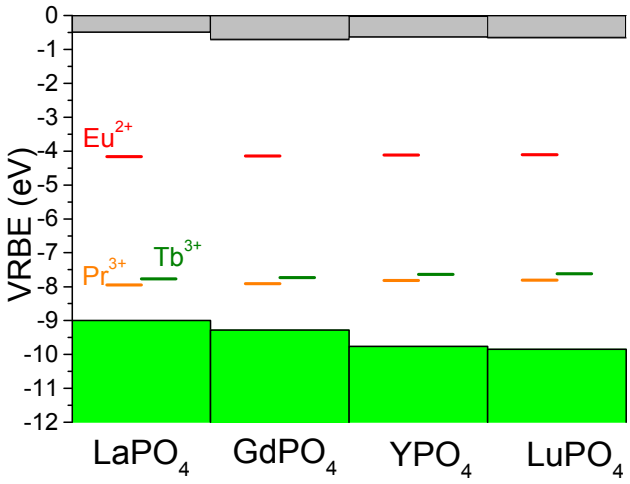

Fig. 2. Stacked VRBE diagram of $REPO_4$ with the binding energy in the ground states of Eu^{2+}, Pr^{3+}, and Tb^{3+}.

2. Experimental

All starting chemicals were purchased from Sigma-Aldrich and used without further treatment. Polycrystals were fabricated by a high temperature solid state reaction. The appropriate stoichiometric mixture of $NH_4H_2PO_4$ (99.99%), La_2O_3 (99.99%), Gd_2O_3 (99.99%), Y_2O_3 (99.99%), Lu_2O_3 (99.999%) and other rare earth oxides (99.999%) were accurately weighted and mixed well in an agate mortar with the help of acetone. The concentrations of the other rare earth oxides were fixed at 0.5 mol %. Afterwards, it was fired in an alumina crucible for 10 h at 1400 ^oC under a reducing atmosphere of H_2/N_2 (H_2:N_2 7%:93%). After cooling, the as-synthesized polycrystals were ground again and fired at 1400 ^oC for another 10 h under the same reducing atmosphere. Finally, the polycrystals were naturally cooled to room temperature, and the obtained compounds were ground into powder before subjecting them to further measurements.

The crystal structures were characterized by a PANalytical XPert PRO X-ray diffraction system with cobalt Kα (λ=0.1788901 nm) X-ray tube at 40 mA and 45 kV. The collected X-ray diffraction (XRD) patterns were compared with reference data derived from the Pearson's Crystal Database. The photoluminescence emission (PL) and PL excitation (PLE) spectra were recorded with equipment that has a UV/VIS branch with a 500 W Hamamatsu CW xenon lamp and Horiba Gemini 180 monochromator, and a VUV/UV branch that is constituted of an ARC VM502 vacuum monochromator and a deuterium lamp (D_2 lamp). Princeton Instruments Acton SP 2300 monochromator and PerkinElmer Photon Counting Module MP1993 were used to disperse and record the emission from the samples. The sample temperature was controlled with a closed-cycle helium (He) cryostat (Model HC-4, APD Cryogenics Inc.) and a temperature controller of Lake Shore 331. All presented excitation curves were corrected for the incident photon flux.

View Article Online
DOI: 10.1039/C7TC05221A

Thermoluminescence (TL) measurements were recorded utilizing a RISØ TL/OSL reader (model DA-15) with DA-20 controller. All samples were irradiated with a $^{90}Sr/^{90}Y$ β source with a dose rate of 0.7 mGy s^{-1} in the TL setup in complete darkness. All TL measurements were performed under a flow of nitrogen gas. Samples with masses <20 mg and area ~0.6 cm^2 were used. For the TL measurements on samples where Ce^{3+} is the recombination center a 3 mm Hoya C5-58 filter in the wavelength range of 350-470 nm was placed between the EMI 9635QA photomultiplier tube (PMT) and the sample to record Ce^{3+} emission only. In order to select the red emission when for example Eu^{3+} is the recombination center, a 600 nm bandpass filter of 600FS40-50 (S250-07) was placed between the PMT and the samples.

For the low temperature TL (LTTL) measurements (90-450 K), the samples were first heated to 450 K for 2 min to empty all relevant traps and then cooled to 90 K followed by 600 s β irradiation with a $^{90}Sr/^{90}Y$ β source at a dose rate of 0.4 mGy s^{-1}. LTTL recordings were measured at the heating rate of 1 K/s in a sample chamber operating under vacuum (10^{-7} mbar) monitoring Eu^{3+} red emission with a PerkinElmer channel photomultiplier tube (MP-1393),. Liquid nitrogen was utilized as a cooling medium.

Prior to the recording the TL emission (TLEM) spectra, the samples were heated to 900 K 3 times to empty all relevant traps and then exposed to γ-ray irradiation from a ^{60}Co source to charge the traps. Emission was recorded with a UV/vis spectrometer (Ocean Optics, model QE65000) in the 200-900 nm range, and a near-infrared (NIR) spectrometer (Ocean Optics, model NIRQ512) in the 900-1700 nm range. Both spectrometers have a high-resolution composite grating of 300 lines/mm and an 100 mm entrance aperture, leading to wavelength resolution of full width at half maximum (FWHM) of 3.3 nm.

TL excitation (TLE) spectra were recorded by means of first illuminating samples during 2400 s using a monochromatic photon beam from a 150 W xenon lamp (Hamamatsu L2273) filtered by a monochromator (Oriel Cornerstone 130). The system was operated under Labview™ allowing the collection of multiple TL glow curves from room temperature to 720 K at heating rate of 5 K/s with changing illumination wavelength. The wavelength step is 10 nm, and the slit width was set at 0.1 cm resulting in a spectrum resolution of 8 nm. The plot of the integrated TL glow curve versus the excitation wavelength is called the TL excitation spectrum[24]. To collect Eu^{3+} emission a 600 nm bandpass filter of 600FS40-50 was placed between the PMT and the samples.

3. Results

3.1. X-ray diffraction and photoluminescence spectroscopy

Fig. 3 shows part of the XRD patterns of $Gd_{1-x}La_xPO_4$:0.005Ce^{3+},0.005Ho^{3+} (x=0-1) solid solutions. $GdPO_4$ and $LaPO_4$ have the same crystal structure with space group $P12_1/c1$. Compared to pure $GdPO_4$ the diffraction peaks show a slight shift towards smaller 2θ angles because the lanthanum ions enter into the smaller gadolinium sites and increase the cell volume. Similar solid solutions were prepared for $Y_{1-x}Lu_xPO_4$:0.005Eu^{3+},0.005Tb^{3+} and the XRD patterns shown in Fig. S1 agree with that in Levushkina et al.[25]

View Article Online
DOI: 10.1039/C7TC05221A

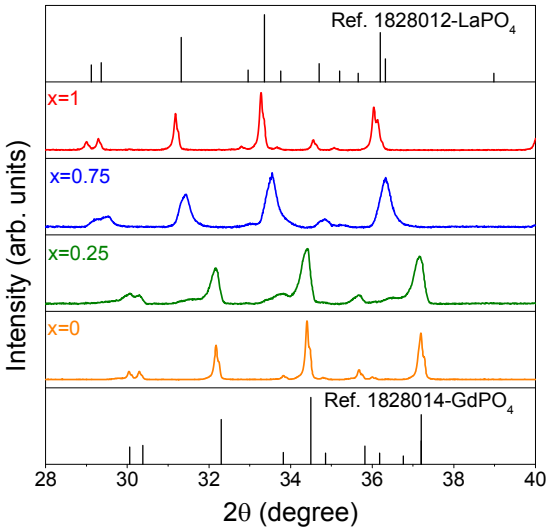

Fig. 3. XRD patterns in the range from 28 to 40° for $Gd_{1-x}La_xPO_4$:0.005Ce^{3+},0.005Ho^{3+} solid solutions.

Fig. 4 shows the VUV excitation spectra of 590 nm Eu^{3+} emission in $REPO_4$: 0.005Eu^{3+},0.005Tb^{3+} at 10 K. The shortest wavelength peak is due to host exciton creation. Its energy E^{ex} increases from 8.05 eV for $LaPO_4$ to 8.67 eV for $LuPO_4$ which agrees with previous reports, i.e., 8.00 eV for $LaPO_4$[22] and 8.60 eV for $LuPO_4$[26].

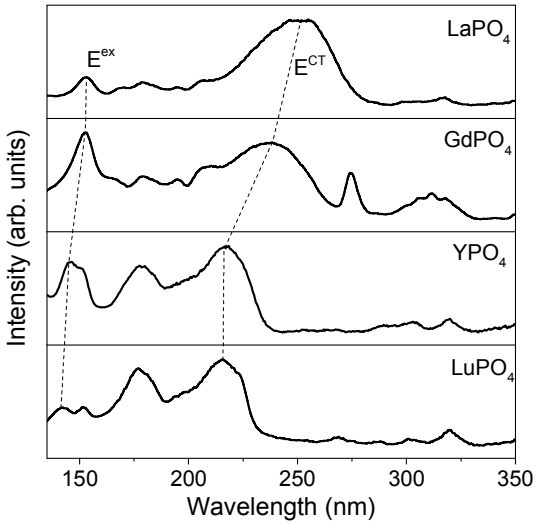

Fig. 4. Photoluminescence excitation (PLE) spectra (λ_{em}=590 nm) of $REPO_4$:0.005Eu^{3+}, 0.005Tb^{3+} (RE=La, Gd, Y, and Lu) samples at 10 K.

The broad excitation bands near 200-260 nm are due to electron transfer from the valence band to Eu^{3+} which are known as the charge transfer (CT) bands. The energy E^{CT} at the maximum of the CT-band increases from 4.88 eV for $LaPO_4$ to 5.76 eV for $LuPO_4$. These

View Article Online
DOI: 10.1039/C7TC05221A

CT-energies are similar to those in literature: e.g., 4.84 eV for $LaPO_4$ and 5.74 eV for $LuPO_4$[22, 27].

3.2. Engineering the electron trap depth

A series of $LaPO_4$:0.005Ce^{3+},0.005Ln^{3+} samples was prepared to demonstrate electron trap depth engineering. All samples are of single phase as demonstrated in the XRD spectra of Fig. S1. Fig. 5 shows the normalized TL glow curves. Each of the Ln^{3+} codopants induces a TL glow at different temperature T_m as listed in column 2 of Table 1.

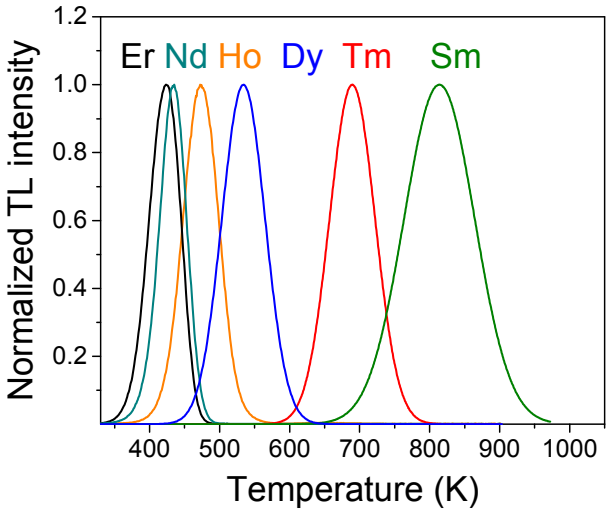

Fig. 5. Normalized TL glow curves of $LaPO_4$:0.005Ce^{3+},0.005Ln^{3+} at heating rate β=5 K/s while monitoring the Ce^{3+} 5d-4f emission.

Table 1. TL results on $LaPO_4$:0.005Ce^{3+},0.005Ln^{3+} showing T_m (K), and the trap depths E (eV) derived from the variable heating rate plot.

Ln	T_m	E
Nd	434	1.08
Sm	817	2.07
Dy	535	1.34
Ho	474	1.18
Er	424	1.05
Tm	690	1.74

View Article Online
DOI: 10.1039/C7TC05221A

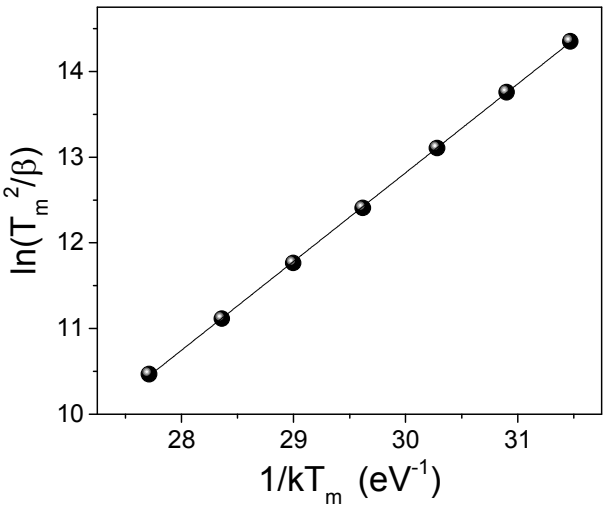

Fig. 6. Variable heating rate plot of $LaPO_4$:0.005Ce^{3+},0.005Er^{3+}. The used heating rates were 0.08, 0.15, 0.30, 0.63, 1.25, 2.5, and 5 K/s.

Assuming first-order TL-recombination kinetics, the trap depth can be determined from a variable heating rate plot using the relation[28-31]

$$\ln\left(\frac{T_m^{\,2}}{\beta}\right) = \frac{E}{kT_m} + \ln\left(\frac{E}{ks}\right) \qquad (1)$$

where β is the heating rate (K/s), k is the Boltzmann constant (eV/K), and s is the frequency factor (s^{-1}). Fig. 6 shows the variable heating rate plot for $LaPO_4$:0.005Ce^{3+},0.005Er^{3+}. For the trap depth a value of 1.05 eV is obtained from the slope of the line through the data and for the frequency factor a value of 1.02×10^{12} s^{-1} is obtained from the intercept with the vertical axis. Since all Ln^{3+} codopants locate at the La^{3+} site, we will assume that the frequency factor s remains a constant.[7, 32] The trap depths for the other codopants then Er^{3+} were determined by using T_m from column 2 of Table 1 and solving Eq. (1) with β=5 K/s. The trap depths are shown in column 3 of Table 1.

Fig. 7a shows the normalized TL glow curves for $Gd_{1-x}La_xPO_4$:0.005Ce^{3+},0.005Ho^{3+} solid solutions. T_m gradually shifts towards higher temperature with increasing x. The TL glow peak for x=0.25 becomes most broad. From variable heating rate plot fits for x=0, 0.5, 0.75, and 1, as can be found in Fig. S2, the trap depths and the frequency factors that are compiled in Table 2 were derived.

View Article Online
DOI: 10.1039/C7TC05221A

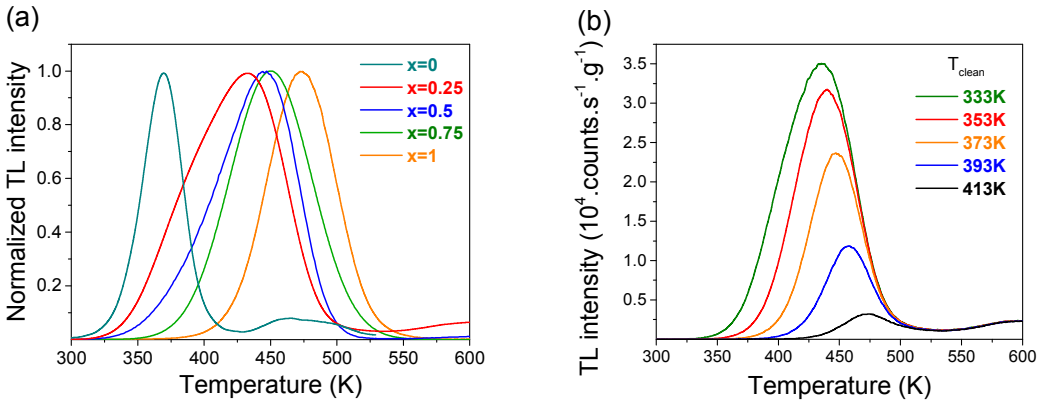

Fig. 7. (a) Normalized TL glow curves of $Gd_{1-x}La_xPO_4$:0.005Ce^{3+},0.005Ho^{3+} solid solutions at β=5 K/s. (b) TL glow curves for x=0.25 after a peak cleaning at T_{clean}.

Table 2. TL results on $Gd_{1-x}La_xPO_4$:0.005Ce^{3+},0.005Ho^{3+} solid solutions listing the T_m (K), and the trap depth E (eV), and frequency factor s (s^{-1}) as obtained from variable heating rate plots. The data for x=0.25 is from the peak cleaning and the initial rise method.

x	T_m	E	s
0	369	0.84	9.53×10^{10}
0.25	432	0.95-1.20	
0.5	445	1.10	3.58×10^{12}
0.75	451	1.16	2.51×10^{12}
1	474	1.22	2.95×10^{12}

To study the glow peak broadening of the sample with x=0.25 we have applied the peak cleaning technique[33]. After exposure to the β source for 200 s at room temperature, the sample is heated to different peak clean temperature (T_{clean}) and kept at that temperature for 400 s. Subsequently a TL recording at a heating rate of 5 K/s is made. Fig. 7b shows that with the increase of T_{clean}, the TL intensity decreases and T_m increases. This shows the presence of a trap depth distribution for the sample with x=0.25, and the increase of T_m is due to the fact that the electrons trapped at shallow traps are liberated at T_{clean} and only the deeper traps remain occupied. The trap depth against T_{clean} can be found by using the initial rise method as explained in the supplementary information in Fig. S3. The trap depth varies between 0.9 and 1.2 eV as shown column 3 of Table 2. Also for x=0.5 and 0.75 there is peak broadening related to a trap depth distribution and the energies in column 3 of Table 2 should be regarded as an average trap depth then.

3.3. Engineering hole release in Y-Lu phosphate solid solutions

Fig. 8 shows the TL emission (TLEM) plots for YPO_4:0.005Eu^{3+},0.005Tb^{3+}, YPO_4:0.005Sm^{3+},0.005Tb^{3+}, YPO_4:0.005Yb^{3+},0.005Tb^{3+}, and YPO_4:0.005Yb^{3+}. Additional TL emission plots for other $REPO_4$ with other combinations of Ln^{3+} doping can be found in Fig. S4.

View Article Online
DOI: 10.1039/C7TC05221A

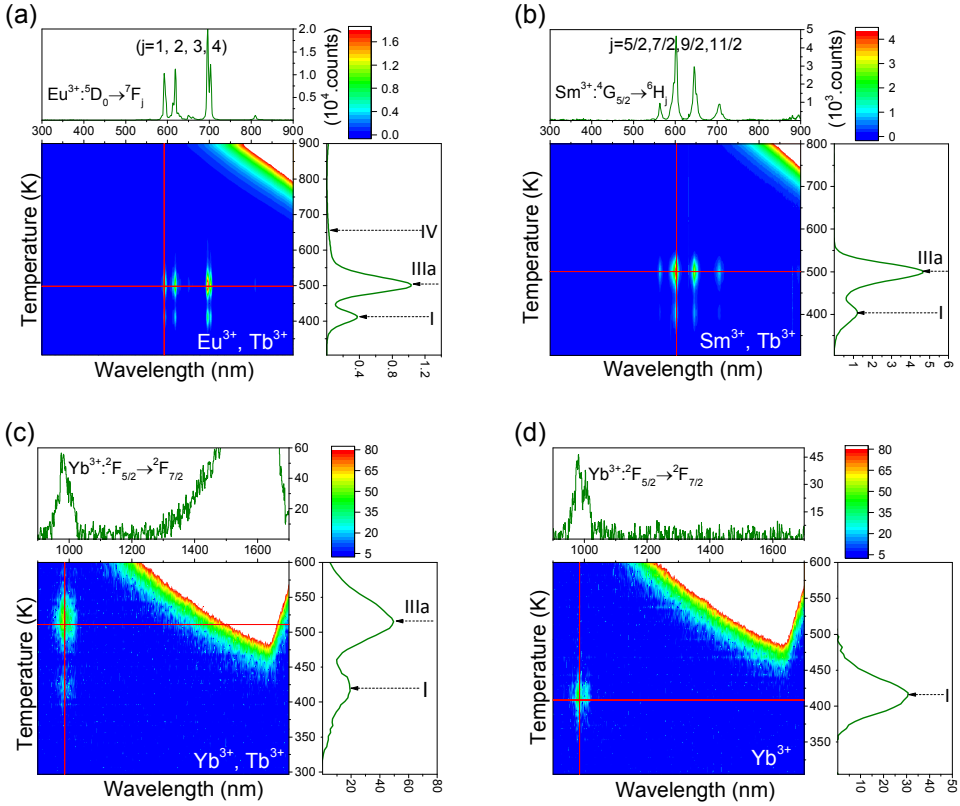

Fig. 8. Thermoluminescence emission (TLEM) spectra of (a) YPO_4:0.005Eu^{3+},0.005Tb^{3+}, (b) YPO_4:0.005Sm^{3+},0.005Tb^{3+}, (c) YPO_4:0.005Yb^{3+},0.005Tb^{3+}, and (d) YPO_4:0.005Yb^{3+} at the heating rate of 1 K/s.

The glow peak at ~507 K for YPO_4:0.005Eu^{3+},0.005Tb^{3+}, which will be referred to as peak IIIa, is also observed for YPO_4:0.005Sm^{3+},0.005Tb^{3+} in Fig. 8b and YPO_4:0.005Yb^{3+}, 0.005Tb^{3+} in Fig. 8c. From the studies by Bos et al. [35] on YPO_4:0.005Sm^{3+},0.005Tb^{3+} and YPO_4:0.005Tm^{3+},0.005Tb^{3+} this glow peak was attributed to hole release from Tb^{4+}. Note that characteristic luminescence originating from Tb^{3+} is absent in Fig. 8 but characteristic emission from either Eu^{3+}, Sm^{3+}, or Yb^{3+} is observed. This applies to YPO_4 but equally well to the other $REPO_4$ in Fig. S4.

The effect of replacing Tb^{3+} for Pr^{3+} or for Ce^{3+} is shown in the TL glow curves of Fig. 9a and 9b. Information on TLEM can be found in Fig. S4. Pr^{3+} gives a glow peak, hereafter referred to as peak IIIb, that is at 10 K lower temperature than peak IIIa for Tb^{3+}. The glow peak is absent when Ce^{3+} is the co-dopant or in case of absence of co-dopants. The VRBE diagram of Fig. 1 predicts that Tb^{3+} and Pr^{3+} provide about the same hole trapping depth and therefore peak IIIb is attributed to hole release from Pr^{4+}. From the variable heating rate plot of YPO_4:Eu^{3+},Tb^{3+} we derived a frequency factor of 1.45×10^{13} s^{-1} for hole release from Tb^{4+}. We assumed that the same value applies for hole release from Pr^{4+}, and then by using the observed T_m in Fig. 9 and Eq. (1) trap depths are derived as shown in Table 3.

Glow peak I is despite different sets of lanthanide dopants present in all TL-spectra of Fig. 9a and 9b. Its origin is not lanthanide related. We attribute it to hole release from unknown

View Article Online
DOI: 10.1039/C7TC05221A

defects. The same applies to glow peaks II and IV that are present when Eu^{3+} is used as deep electron trap.

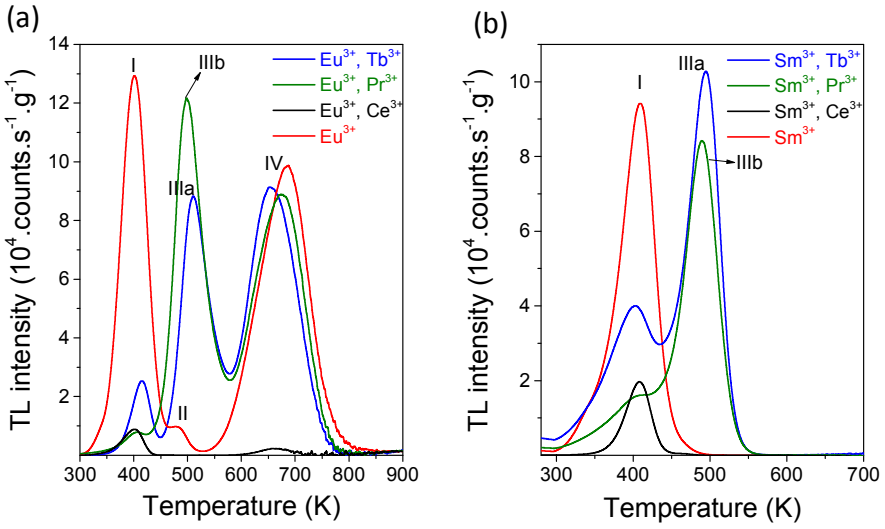

Fig. 9. TL glow curves of (a) YPO_4:0.005Eu^{3+},0.005Ln^{3+} and (b) YPO_4:0.005Sm^{3+},0.005Ln^{3+} recorded after 2000 s β source radiation monitoring the emission from Eu^{3+} or from Sm^{3+} at the heating rate of 1 K/s.

Table 3. TL results for $REPO_4$:0.005Ln^{3+},Tb^{3+} or Pr^{3+} providing the trap depths E (eV) for the glow peaks IIIa and IIIb, and the frequency factor s (s^{-1}).

Compound	s	Ln^{3+}	Tb E(IIIa)	Pr E(IIIb)
YPO_4	1.45×10^{13}	Eu^{3+}	1.45	1.41
YPO_4	1.45×10^{13}	Sm^{3+}	1.42	1.40
YPO_4	1.45×10^{13}	Yb^{3+}	1.46	1.46
$Y_{0.75}Lu_{0.25}PO_4$	4.45×10^{13}	Eu^{3+}	1.52	1.50
$Y_{0.5}Lu_{0.5}PO_4$	2.53×10^{14}	Eu^{3+}	1.65	1.63
$Y_{0.5}Lu_{0.5}PO_4$	2.53×10^{14}	Yb^{3+}	1.62	1.61
$Y_{0.25}Lu_{0.75}PO_4$	1.29×10^{15}	Eu^{3+}	1.78	1.75
$LuPO_4$	1.03×10^{15}	Eu^{3+}	1.84	1.80
$LuPO_4$	1.03×10^{15}	Yb^{3+}	1.79	1.78
$LaPO_4$	2.14×10^{12}	Eu^{3+}	0.63	0.55

Fig. 10 shows the TL glow curves for $Y_{1-x}Lu_xPO_4$:0.005Eu^{3+},0.005Tb^{3+} solid solutions. With increasing x, peak IIIa shifts from 507 towards 572 K. The trapping parameters were derived using the variable heating rate plots[13] in Fig. S6, and results are compiled in Table 3. TL glow curves for $Y_{1-x}Lu_xPO_4$:0.005Eu^{3+},0.005Pr^{3+} solid solutions can be found in Fig. S7. Like peak IIIa for Tb^{3+}, peak IIIb for Pr^{3+} shifts from 494 towards 560 K with increasing x. The derived trapping parameters are shown in Table 3.

View Article Online
DOI: 10.1039/C7TC05221A

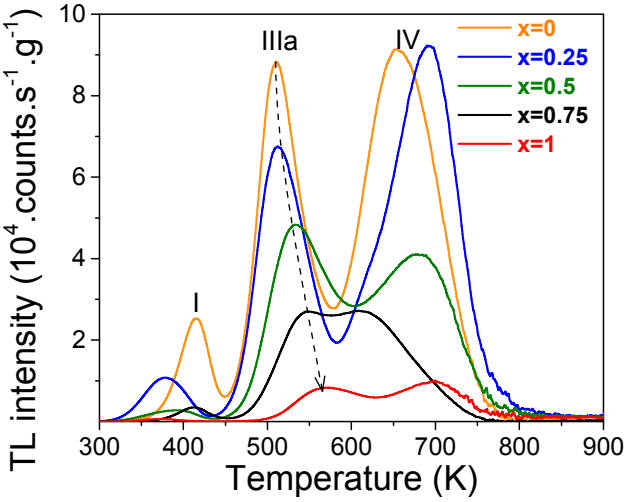

Fig. 10. TL glow curves for $Y_{1-x}Lu_xPO_4$:0.005Eu^{3+},0.005Tb^{3+} solid solutions monitoring the red emission from Eu^{3+} at the heating rate of 1 K/s.

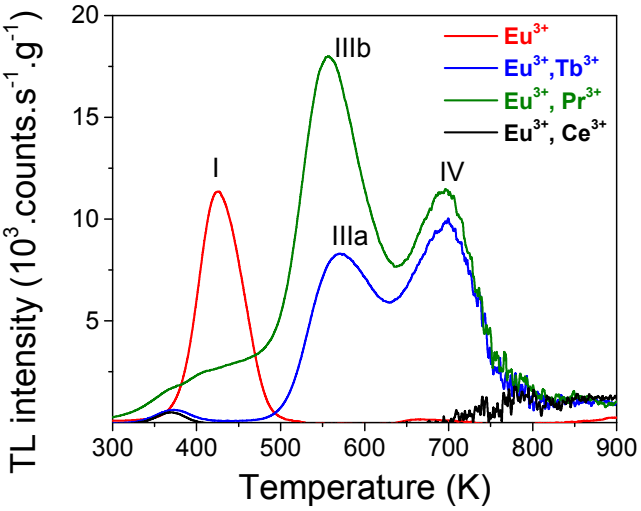

Fig. 11. TL glow curves for $LuPO_4$:0.005Eu^{3+},0.005Ln^{3+} (Ln=Tb, Pr, and Ce) samples monitoring the red emission from Eu^{3+} at the heating rate of 1 K/s.

Fig. 11 compares the TL glow curves of $LuPO_4$:0.005Eu^{3+},0.005Ln^{3+}. Similar as in Fig. 9, the glow peak IIIb for hole release from Pr^{4+} appears at about 10 K lower temperature than that from Tb^{4+}, and also glow peaks I and IV seem to be present. The TL glow curves of the single Eu^{3+} and the Eu^{3+},Ce^{3+}-codoped samples are shown to demonstrate the absence of peaks IIIa and IIIb.

Fig. 12 shows the low temperature TL (LTTL) glow curves of $LaPO_4$:0.005Eu^{3+}, 0.005Ln^{3+}. Similar as in Fig. 9 and 11, Pr gives rise to an additional glow peak below RT denoted as IIIb and Tb^{3+} to a glow peak IIIa at about 30 K higher temperature. The TL glow

View Article Online
DOI: 10.1039/C7TC05221A

curve of the $LaPO_4:Eu^{3+},Ce^{3+}$ is shown to demonstrate the absence of peaks IIIa and IIIb. The glow peaks appearing above room temperature were further also studied with the Riso reader as shown in Fig. S8. The variable heating rate plot for glow peak IIa of $LaPO_4:0.005Eu^{3+},0.005Tb^{3+}$ as shown in Fig. S8b provides the trapping parameters. By assuming a similar frequency factor for glow peaks IIIa and IIIb the activation energies compiled in Table 3 were estimated.

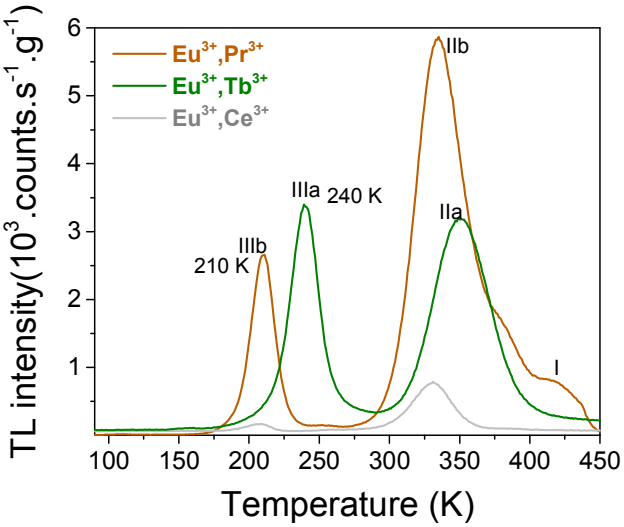

Fig. 12. TL glow curves for $LaPO_4:0.005Eu^{3+},0.005Ln^{3+}$ (Ln=Tb, Pr, and Ce) samples monitoring the Eu^{3+} emission in the temperature range of 90-450 K at the heating rate of 1 K/s.

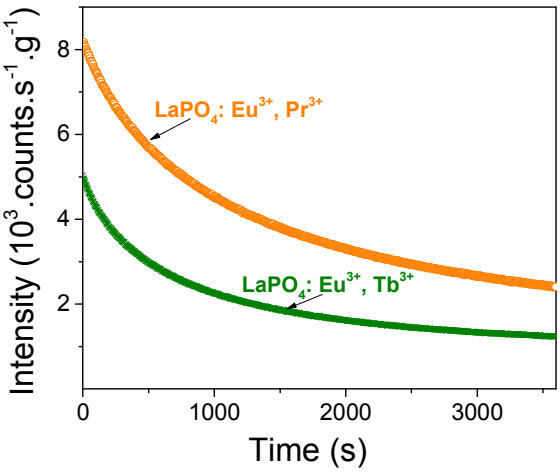

Fig. 13. Room temperature isothermal decay curves of $LaPO_4:0.005Eu^{3+},0.005Tb^{3+}$ and $LaPO_4:0.005Eu^{3+},0.005Pr^{3+}$. A 600 nm bandpass filter (600FS40-50) was used to monitor the red emission of Eu^{3+}.

View Article Online
DOI: 10.1039/C7TC05221A

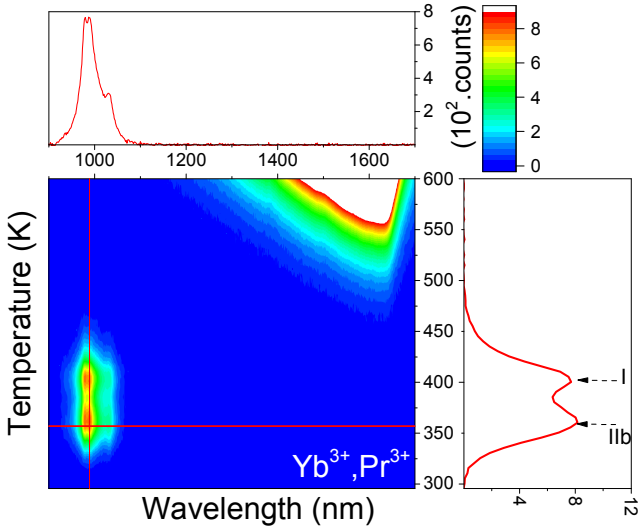

Fig. 14. TL emission (TLEM) spectrum for $LaPO_4$:0.005Yb^{3+},0.005Pr^{3+}.

Because of the intense glow peaks near room temperature in the $LaPO_4$ samples we measured the room temperature isothermal decay curves as shown in Fig. 13. $LaPO_4$:0.005Eu^{3+},0.005Pr^{3+} with the most intense glow peak also shows the most intense afterglow.

For $LaPO_4$:0.005Eu^{3+},0.005Tb^{3+} and $LaPO_4$:0.005Eu^{3+},0.005Pr^{3+} we have red afterglow from Eu^{3+}. Fig. 14 shows the TL emission (TLEM) spectrum of $LaPO_4$:0.005Yb^{3+},0.005Pr^{3+} where the emission is from Yb^{3+} at 1000 nm in the short wavelength infrared (SWIR) 900-1700 nm range. Additional TL emission plots for other $REPO_4$ with combinations of Yb^{3+} and Tb^{3+} or Pr^{3+} can be found in Fig. S4i-S4l and in each case IR Yb^{3+} TL-glow is observed. Infrared persistent luminescence from Yb^{3+} appears in $LaPO_4$:0.005Yb^{3+},0.005Pr^{3+} and $LaPO_4$:0.005Yb^{3+},0.005Tb^{3+} at room temperature.

The room temperature afterglow of $LaPO_4$:0.005Eu^{3+},0.005Tb^{3+} and $LaPO_4$: 0.005Eu^{3+},0.005Pr^{3+} is related to the lowest temperature glow peak. To study the origin of this glow peak Fig. 15 shows the TL excitation (TLE) spectrum of the low temperature glow peak at 300-380 K of $LaPO_4$:0.005Eu^{3+},0.005Tb^{3+}. A broad TLE band ranging from 200 to 300 nm and peaking at 260 nm is observed. The width and position is similar as that of the photoluminescence excitation (PLE) spectrum of Eu^{3+} single doped $LaPO_4$ also shown in Fig. 15. This demonstrates that after Eu^{3+} CT-band excitation, the holes that are generated in the valence band are trapped by the defects responsible for the low temperature glow peak.

View Article Online
DOI: 10.1039/C7TC05221A

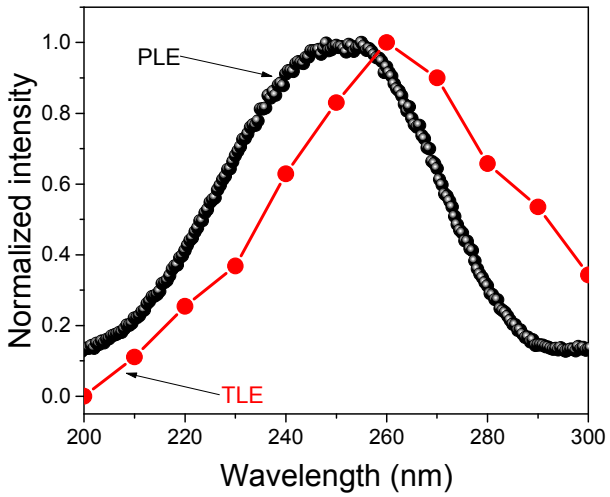

Fig. 15. Thermoluminescence excitation (TLE) spectrum of $LaPO_4$:0.005Eu^{3+},0.005Tb^{3+} and photoluminescence excitation (PLE) spectrum (λ_{em}=590 nm) of $LaPO_4$:0.005Eu^{3+} performed at room temperature.

4. Discussion

The vacuum referred binding energy (VRBE) diagrams shown in Fig. 1 are first discussed, and then we will show how they can be used for tailoring the trapping and release process of electrons and holes in $REPO_4$. The energy of an electron at rest in vacuum is defined as the reference energy, i.e., energy zero[18]. VRBE is defined as the energy needed to extract an electron from a system and bring it to the vaccum[16, 17]. This electron can be from a host band or from an impurity ground or excited state.

Table 4. Parameters used to establish the VRBE diagrams for $REPO_4$ (RE=La, Gd, Y, and Lu) in eV and the results from these diagrams.

$REPO_4$	U	E_{Eu}^{2+}	$E_{Eu}^{3+,CT}$	E_V	E^{ex}	E_C	E_{Tb}^{3+}	E_{Pr}^{3+}
La	7.18	-4.16	4.84	-9.00	8.0	-0.49	-7.77	-7.95
Gd	7.15	-4.15	5.14	-9.28	8.0	-0.71	-7.73	-7.91
Y	7.09	-4.12	5.65	-9.77	8.5	-0.63	-7.64	-7.82
Lu	7.08	-4.11	5.74	-9.85	8.6	-0.66	-7.62	-7.80

To construct VRBE diagrams, one first needs the values for the U-parameter that are listed in column 2 of Table 4. The U-parameters were derived already for $REPO_4$ (RE=La, Y and Lu) in Ref. [22] and for $GdPO_4$ it is estimated. From these values the VRBE in the Eu^{2+} ground state is calculated with the chemical shift model and results are shown in column 3 of Table 4. The VRBE at the valence band top shown in column 5 can be obtained employing the VB→Eu^{3+} CT-energy as measured in Fig. 4 and given in column 4. The VRBE E_C at the conduction band bottom shown in column 7 of Table 4 is obtained from the host exciton

View Article Online
DOI: 10.1039/C7TC05221A

creation energy E^{ex} in column 6 by adding the exciton binding energy estimated as $0.008(E^{ex})^2$ in Ref.[19]. We will use the most recent parameter sets from Ref.[19] to construct the double zigzag curves which then provide the VRBE in divalent lanthanide ground states and trivalent ground states as listed for Tb and Pr in columns 8 and 9.

4.1. Electron trap depth tailoring via conduction band engineering

Fig. 5 showed that T_m strongly depends on the type of the lanthanide in $LaPO_4$: $0.005Ce^{3+}$,$0.005Ln^{3+}$. A similar dependence was reported for $GdAlO_3$:$0.01Ce^{3+}$,$0.01Ln^{3+}$[7], $Y_3Al_5O_{12}$:$0.003Ce^{3+}/Pr^{3+}/Tb^{3+}$,$0.003Ln^{3+}$[34], and YPO_4:$0.005Ce^{3+}$,$0.005Ln^{3+}$[35]. Using the derived electron trap depths as listed in column 3 of Table 1 we have placed the Ln^{2+} ground state levels below the conduction band in the VRBE diagram of Fig. 16a. Apart from a deviation of 0.1-0.4 eV the data from TL glow peak analysis follow the divalent lanthanide zigzag curve in the VRBE diagram.

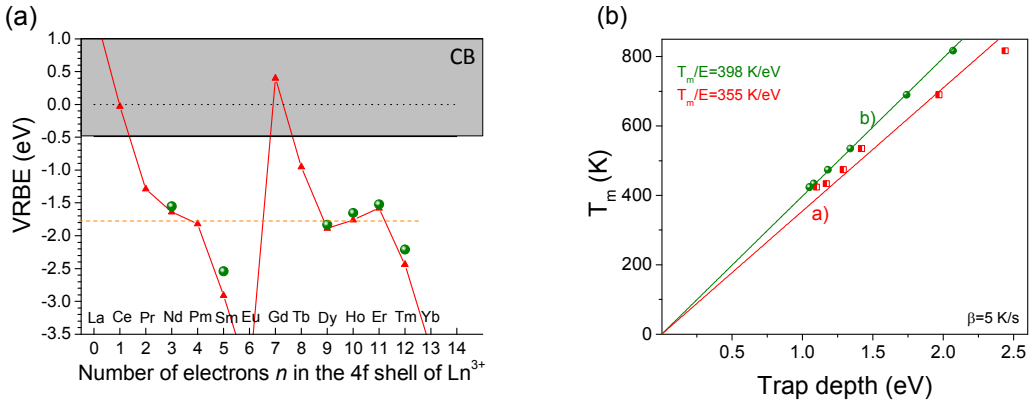

Fig. 16. (a) VRBE-diagram for the divalent lanthanides in $LaPO_4$ (▲) together with VRBE data from TL-studies on $LaPO_4$:$0.005Ce^{3+}$,$0.005Ln^{3+}$ (●). (b) T_m against the trap depth as line a) determined from the VRBE diagram and line b) from TL studies on $LaPO_4$:$0.005Ce^{3+}$, $0.005Ln^{3+}$.

Fig. 16b shows T_m from Fig. 5 for $LaPO_4$:$0.005Ce^{3+}$,$0.005Ln^{3+}$ against the trap depths read from the VRBE diagram and against the trap depths derived by TL glow peak analysis. Proportional relationships are observed with the slope T_m/E=355 K/eV and 398 K/eV, respectively. Assuming first order TL-recombination kinetics Eq. (1) can also be written as

$$\frac{T_m}{E} = \frac{11600}{\ln\left(\frac{T_m}{E}\right) + \ln\left(\frac{s}{\beta}\right) + \ln\left(T_m\right) - 9.36} \quad \text{K/eV} \qquad (2)$$

The frequency factor s in inorganic compounds is typically 10^{13} s^{-1} and $\ln\left(\frac{s}{\beta}\right)$ is then 28.3 for β=5 K/s. $\ln\left(\frac{T_m}{E}\right)$ and $\ln\left(T_m\right)$ are both near 6 which then implies that the value for the

View Article Online
DOI: 10.1039/C7TC05221A

enumerator in Eq. (2) is about 31 and almost entirely determined by $\ln(\frac{s}{\beta})$. It also implies that $\frac{T_m}{E}$ will be to good approximation a constant with values of 300-400 K/eV depending on $\ln(\frac{s}{\beta})$ as observed. Proportional relations were also reported for lanthanides in YPO_4[35], $CaSO_4$[36], and $Sr_3Al_xSi_{1-x}O_5$[37] with T_m/E=284 K/eV at β=0.1 K/s, T_m/E=313 K/eV at β=0.42 K/s, and T_m/E=322 K/eV at β=0.1 K/s, respectively. Particularly, for YPO_4 T_m/E=300 K/eV was obtained at β=1 K/s. Fig. 11b also shows that the two fitted lines a) and b) deviate. Clearly, taking into account the error by VRBE and considering that there is an uncertainty in the slope of the line based on the thermoluminescence measurements as well, the trend is in accordance.

Fig. 2, that was made with the data from Table 4, shows the stacked vacuum referred binding energy (VRBE) diagram of $REPO_4$ with the VRBE in the $4f^n$ ground states of Pr^{3+}, Tb^{3+}, and Eu^{2+}. The VRBE diagrams with all lanthanide impurity level locations can be found in Fig. S9. The conduction band bottom moves 0.22 eV downward with the substitution of La^{3+} by Gd^{3+} in $Gd_{1-x}La_xPO_4$ solid solutions (column 7 of Table 4) and then the Ln^{3+} electron trap depths will decrease. This is consistent with the 105 K TL peak shift in Fig. 7a. The same sequence of TL glow peaks of the same Ln^{3+} dopant as in Fig. 5 was observed for YPO_4:Ce^{3+},Ln^{3+} at the same heating rate of 5 K/s in Ref. [35]. All glow peaks in YPO_4 are shifted 90-100 K towards lower T_m, as shown in Fig. S10. Assuming T_m/E~350 K/eV this corresponds with 0.26 eV more shallow trap depth in YPO_4 whereas Fig. 2 and Table 4 predict 0.18 eV more shallow trap depth.

From the almost 100 K broad TL glow peak observed for x=0.25 in Fig. 7a, a 0.95-1.2 eV wide electron trap depth distribution was found (see Table 2). Apparently the VRBE at the conduction band bottom shows site-to-site fluctuations depending on the statistics in replacing La by Gd in the $Gd_{1-x}La_xPO_4$ solid solution at x=0.25. A similar phenomenon was reported for Eu^{3+}-doped SnO_2 nanoparticles[38] and $Y_3Al_{5-x}Ga_xO_{12}$:Ce^{3+},Cr^{3+} solid solutions when changing the ratio of Ga^{3+} to Al^{3+}[13].

4.2. Controlling the hole trap depth

The vacuum referred binding energy (VRBE) diagrams of $REPO_4$ in Fig. 1 and Fig. S9 predict that the holes trapped by Tb^{4+} and Pr^{4+} will be liberated earlier, i.e., at lower temperature than the electrons trapped at the Eu^{2+}, Yb^{2+}, and Sm^{2+} to generate the characteristic 4f-4f emission of Eu^{3+}, Yb^{3+}, and Sm^{3+}.

The room temperature TL excitation spectrum for $LaPO_4$:$0.005Eu^{3+}$,$0.005Tb^{3+}$ in Fig. 15 strongly resembles with the VB→Eu^{3+} CT band in Fig. 4, i.e., the width is the same but it appears 10 nm redshifted corresponding with 0.2 eV. During CT-band excitation holes are generated in the valence band[2, 7] and this is usually followed by the back transfer of the electron from Eu^{2+} generating Eu^{3+} emission. Struck et al. reported on the phenomenon of hole separation from the Eu^{3+} CT-state in RE_2O_2S (RE=Y^{3+} and La^{3+}) during Eu^{3+}-CT

View Article Online
DOI: 10.1039/C7TC05221A

excitation[39]. Dobrov et al. reported that a p-type photoconductivity signal was found in La_2O_2S:Eu during the VB→Eu^{3+} CT excitation[40]. Therefore, during CT-band excitation holes can be liberated from the CT-state and subsequently migrate to hole trapping centers that can be host intrinsic defects or intentional defects such as Tb^{3+} and Pr^{3+}. Fig. 15 suggests that this occurs in $LaPO_4$: $0.005Eu^{3+}$,$0.005Tb^{3+}$ and that the close to room temperature glow peak in Fig. 12 must be attributed to the release of holes from either Tb^{4+} or an intrinsic defect. The 0.2 eV redshift in band location may indicate that the hole trap is close to Eu^{3+} and thus facilitating the hole release.

Fig. 8a-8c showed TL emission (TLEM) spectra for YPO_4 each with the same Tb^{3+} hole trapping center but with different deep electron trapping centers of Eu^{3+}, Sm^{3+}, and Yb^{3+}. All samples share TL glow peaks I and IIIa with emission from either Eu^{3+}, Sm^{3+} or Yb^{3+}. Peak IIIa was assigned to hole release from Tb^{4+}. Peak I is also observed when the Tb^{3+} hole trap is replaced by the Pr^{3+} or Ce^{3+} hole trap in the samples of Fig. 9 and S4. We therefore attribute peak I to hole release from an unidentified host associated hole trap. Glow peak IV in Fig. 9a, is only observed in Eu^{3+}-doped samples and it seems to be a further unidentified hole trap somehow related to Eu presence.

Using data in columns 4 and 5 of Table 3 the average trap depths for Pr^{3+} and Tb^{3+} in YPO_4 are 1.42 and 1.44 eV, which are ~0.6 eV smaller than the predicted ones from the VRBE diagram (1.95 for Pr^{3+} and 2.13 eV for Tb^{3+}). A similar deviation was observed in $GdAlO_3$[7]. When holes are produced in the valence band they trend to form a V_k center by bonding two neighbouring oxygen anions[41, 42]. In a VRBE diagram such V_k center level is then located above the valence band top[7, 43]. We therefore attribute the 0.6 eV energy difference to the binding energy of the V_k center. Under thermal excitation, such V_k center moves towards the electron trapped at Yb^{2+}, Sm^{2+}, or Eu^{2+} producing 4f-4f emission of Yb^{3+}, Sm^{3+}, or Eu^{3+} in YPO_4.

4.3. Hole trap depth tailoring via valence band engineering

Since the VRBE in the Tb^{3+} and Pr^{3+} ground states in our phosphate compounds are about the same, the hole trap depths of Tb^{3+} and Pr^{3+} will depend on the VRBE at the valence band top (E_V). Therefore one can tailor the T_m of glow peaks IIIa and IIIb by engineering the VRBE at the valence band top. The stacked diagram in Fig. 2 and column 5 in Table 4 show that E_V lowers by 0.85 eV in discrete steps in going from La- to Gd- to Y- to Lu-phosphate, and the hole trapping depths and T_m of peaks IIIa and IIIb should increase accordingly.

The results on the $Y_{1-x}Lu_xPO_4$ solid solutions in Fig. 10 and S7 demonstrate this tailoring. For both Tb and Pr glow peaks IIIa and IIIb shift upward about 65 K when replacing Y^{3+} by Lu^{3+}. Using a T_m/E relationship of typical 350 K/eV this would imply 0.2 eV deeper hole trap depth. From the variable heating rate plots for $Y_{1-x}Lu_xPO_4 0.005Eu^{3+}$,$0.005Tb^{3+}$ in Fig. S6 about 0.4 eV deeper hole trapping depth is found. The VRBE results in Table 4 suggest only 0.1 eV larger trapping depth. This all demonstrates the limitations in accuracy of trapping depths derived from TL glow curve analysis and VRBE diagram. The VRBE diagram that is based on wide CT-band transitions and other experimental input parameters can easily contain errors of several 0.1 eV size, and this same applies for results from TL data. For example, for

View Article Online
DOI: 10.1039/C7TC05221A

$LaPO_4$:0.005Ce^{3+},0.005Ho^{3+} electron trap of 1.18 eV is found, but in column 3 of Table 2 for the same sample a value of 1.22 eV is obtained. These differences are directly related to different values for the frequency factors. In this work we analyzed the TL-glow peaks assuming first order recombination kinetics and with zero distribution in trapping depths. Such situation is not realistic and reported trapping depth energies and frequency factors should then be treated as indicative.

The VRBE-diagram of $LaPO_4$ in Fig. 2 and Table 4 predicts that Eu^{3+} can act as a 3.67 eV deep electron trapping center, while Ce^{3+}, Tb^{3+}, and Pr^{3+} as 2.90, 1.23, and 1.05 eV shallow hole trapping centers. Considering that the $LaPO_4$ and YPO_4 compounds are quite similar, we assume that the binding energy of the V_k center in $LaPO_4$ is 0.6 eV like in YPO_4. We then arrive at effective hole trapping depths of 2.30, 0.63, and 0.45 eV for Ce^{3+}, Tb^{3+}, and Pr^{3+}, respectively. One can estimate according to Eq. (1) with a heating rate of 1 K/s and the above predicted trapping depths that hole release from Ce^{4+}, Tb^{4+}, and Pr^{4+} in $LaPO_4$ will give glow peaks at T_m ~840, 240, and 170 K, respectively. Clearly, the Ce^{4+} trap is far too deep to release a hole in the measurement range. In contrast, the predicted T_m values for Tb^{4+} and Pr^{4+} hole release are in the range of the appearance of glow peaks IIIa (0.63 eV) and IIIb (0.55 eV) in Fig. 12. We therefore tentatively attribute glow peaks IIIa and IIIb to hole release from Tb^{4+} and Pr^{4+}. The intense glow peak just above RT is then assigned to intrinsic hole traps.

The VRBE-diagram for La-, and $GdPO_4$ in Fig. 2 and the data in Table 4 suggests that the Tb^{3+} and Pr^{3+} hole trap depth will increase by about 0.3 eV corresponding with about 100 K shift of T_m. The glow peak maxima are then expected between 300-400 K in $GdPO_4$. TL glow curves for $GdPO_4$:0.005Eu^{3+},0.005Ln^{3+} (Ln=Tb, Pr, and Ce) samples indeed shows glow peaks between 300-400 K in Fig. S11. However, since they are also present with Ce^{3+} co-doping and for single Eu^{3+} samples they cannot be assigned to either Tb or Pr. This also applies to $GdPO_4$:0.005Sm^{3+},0.005Ln^{3+}.

The data in Table 4 from the VRBE diagram places the ground state level of Tb^{3+} ~0.18 eV higher than that of Pr^{3+} and release of holes from Tb^{4+} should then occur at 60-70 K higher temperature than from Pr^{4+}. However, Fig. 9, 11, and 12 show that the Pr^{4+} TL glow peak appears at 10-30 K lower temperature than that of Tb^{4+} in Y-, Lu, and $LaPO_4$. For $GdAlO_3$ it was found in Ref. [7] that the Pr^{4+} glow peak is at 10-30 K higher temperature than that of the Tb^{4+}. Based on these observations it seems that the ground states of Tb^{3+} and Pr^{3+} have in those compounds about the same VRBE value. It provides a hint that the parameter values behind the trivalent lanthanide zigzag curve in the VRBE diagrams needs adjustment or otherwise might be slightly compound dependent.

There is an increasing need for afterglow phosphors that exhibit emission in the short-wave infrared (SWIR) spectral region of ~900-1700 nm, owing to many advanced applications in the field of military, anti-counterfeiting, and bio-imaging[44]. For instance, for military utilizations, the SWIR light is more mysterious than near-infrared light, which cannot be easily probed by conventional techniques such as night-vision spectacles. For bio-imaging, SWIR light is located in the second biological window (~1000-1400 nm) allowing ultra-

View Article Online
DOI: 10.1039/C7TC05221A

sensitive and deep-tissue bio-imaging[10]. However, rarely SWIR phosphors are developed since it remains unclear how to design such type of materials[45].

SWIR afterglow can be realized by replacing Eu^{3+} for Yb^{3+} and combining that with Tb^{3+} or Pr^{3+} in La-, Y-, Gd-, and Lu- phosphates or in solid solutions thereof. The VRBE at the VB-top and therewith the Tb^{3+} and Pr^{3+} hole trap depths can then be engineered. The results on the Yb^{3+},Tb^{3+}-codoped YPO_4 in Fig. 8c, $Y_{1-x}Lu_xPO_4$ solid solution in Fig. S4i, and $LuPO_4$ in Fig. S4j demonstrates such engineering.

5. Conclusions

The chemical shift model, photoluminescence spectroscopy and thermoluminescence have been combined to study the trapping and release process of electrons and holes in double lanthanide doped rare earth ortho phosphates. In $LaPO_4$:$0.005Ce^{3+}$,$0.005Ln^{3+}$, the Ln^{3+} codopants act as the electron trapping centers, while Ce^{3+} acts as the luminescence center. The electrons liberated from Ln^{2+} recombine with Ce^{4+} yielding Ce^{3+} 5d-4f emission. The electron trap depth generated by lanthanide codopants can be tuned by the choice of Ln^{3+} lanthanide, and for fixed set of lanthanide dopants like in $Gd_{1-x}La_xPO_4$:$0.005Ce^{3+}$,$0.005Ho^{3+}$ solid solutions by tuning x leading to conduction band engineering. For YPO_4:$0.005Ln^{3+}$,$0.005M^{3+}$ (Ln=Sm, Eu, and Yb; M=Pr and Tb), Ln^{3+} acts as electron trapping center and recombination center, while M^{3+} as hole trapping center. Compared with electrons trapped at Ln^{2+}, holes trapped by M^{4+} liberate at lower temperature and recombine with Ln^{2+} to produce Ln^{3+} 4f-4f emission during TL readout. Vacuum referred binding energy (VRBE) at the valence band top can be engineered though the substitution of Y^{3+} by Lu^{3+} or La^{3+} and this enables the tailoring of hole trap depths of Tb^{3+} and Pr^{3+}, and the emitting wavelength can be tailored from red to SWIR by changing the electron traps from Eu^{3+} or Sm^{3+} to Yb^{3+}. Particularly, new SWIR afterglow phosphors with Yb^{3+} infrared emission in ~900-1700 nm have been discovered by tuning the hole trap depth in the ortho phosphates. With the deep understanding of trap level locations and on the transport and trapping processes of charge carriers, such conduction and valence band engineering could be a promising route to deliberate design the electron and hole traps based novel optical storage and persistent phosphors.

6. Acknowledgements

T. Lyu acknowledges the Chinese Scholarship Council for his Ph.D. scholarship (Tianshuai Lyu: No. 201608320151). We thank Dr Adrie J.J. Bos and Dr Hongde Luo from Delft University of Technology, for fruitful discussions on afterglow phosphors and luminescence mechanisms.

Reference

1. Y. Li, M. Gecevicius and J. Qiu, *Chemical Society Reviews*, 2016, **45**, 2090-2136.
2. H. Luo, A. J. J. Bos and P. Dorenbos, *The Journal of Physical Chemistry C*, 2017, **121**, 8760-8769.
3. T. Wang, W. Bian, D. Zhou, J. Qiu, X. Yu and X. Xu, *The Journal of Physical Chemistry C*, 2015, **119**, 14047-14055.
4. Y. Zhuang, Y. Katayama, J. Ueda and S. Tanabe, *Optical Materials*, 2014, **36**, 1907-1912.

View Article Online
DOI: 10.1039/C7TC05221A

5. P. Leblans, D. Vandenbroucke and P. Willems, *Materials*, 2011, **4**, 1034.
6. Y. Wang, Y. Gong, X. Xu and Y. Li, *Journal of Luminescence*, 2013, **133**, 25-29.
7. H. Luo, A. J. J. Bos and P. Dorenbos, *The Journal of Physical Chemistry C*, 2016, **120**, 5916-5925.
8. A. Jain, A. Kumar, S. J. Dhoble and D. R. Peshwe, *Renewable and Sustainable Energy Reviews*, 2016, **65**, 135-153.
9. H. Guo, Y. Wang, G. Li, J. Liu, P. Feng and D. Liu, *Journal of Materials Chemistry C*, 2017.
10. J. Xu, S. Tanabe, A. D. Sontakke and J. Ueda, *Applied Physics Letters*, 2015, **107**, 081903.
11. Z. Pan, Y.-Y. Lu and F. Liu, *Nat Mater*, 2012, **11**, 58-63.
12. J. Ueda, M. Katayama, K. Asami, J. Xu, Y. Inada and S. Tanabe, *Opt. Mater. Express*, 2017, **7**, 2471-2476.
13. J. Ueda, P. Dorenbos, A. J. J. Bos, K. Kuroishi and S. Tanabe, *Journal of Materials Chemistry C*, 2015, **3**, 5642-5651.
14. K. Korthout, K. Van den Eeckhout, J. Botterman, S. Nikitenko, D. Poelman and P. F. Smet, *Physical Review B*, 2011, **84**.
15. K. Chakrabarti, V. K. Mathur, J. F. Rhodes and R. J. Abbundi, *Journal of Applied Physics*, 1988, **64**, 1363-1366.
16. P. Dorenbos, *Physical Review B*, 2012, **85**, 165107.
17. P. Dorenbos, *Journal of Materials Chemistry*, 2012, **22**, 22344-22349.
18. P. Dorenbos, *ECS Journal of Solid State Science and Technology*, 2013, **2**, R3001-R3011.
19. P. Dorenbos, *Optical Materials*, 2017, **69**, 8-22.
20. P. Dorenbos and E. G. Rogers, *ECS Journal of Solid State Science and Technology*, 2014, **3**, R150-R158.
21. P. Dorenbos, *Journal of Luminescence*, 2014, **151**, 224-228.
22. P. Dorenbos, *J. Phys.-Condes. Matter*, 2013, **25**.
23. P. Dorenbos, *Journal of Luminescence*, 2013, **136**, 122-129.
24. A. J. J. Bos, R. M. van Duijvenvoorde, E. van der Kolk, W. Drozdowski and P. Dorenbos, *Journal of Luminescence*, 2011, **131**, 1465-1471.
25. V. S. Levushkina, D. A. Spassky, E. M. Aleksanyan, M. G. Brik, M. S. Tretyakova, B. I. Zadneprovski and A. N. Belsky, *Journal of Luminescence*, 2016, **171**, 33-39.
26. P. Dorenbos, *Journal of Luminescence*, 2005, **111**, 89-104.
27. E. Nakazawa and F. Shiga, *Journal of Luminescence*, 1977, **15**, 255-259.
28. R. Chen and S. A. A. Winer, *Journal of Applied Physics*, 1970, **41**, 5227-&.
29. W. Hoogenstraaten, *Philips Res. Rep*, 1958, **13**, 515–693.
30. R. R. Haering and E. N. Adams, *Physical Review*, 1960, **117**, 451-454.
31. A. J. J. Bos, *Radiation Measurements*, 2006, **41**, S45-S56.
32. A. J. J. Bos, P. Dorenbos, A. Bessière and B. Viana, *Radiation Measurements*, 2008, **43**, 222-226.
33. K. Van den Eeckhout, A. J. J. Bos, D. Poelman and P. F. Smet, *Physical Review B*, 2013, **87**, 045126.
34. F. You, A. J. J. Bos, Q. Shi, S. Huang and P. Dorenbos, *Physical Review B*, 2012, **85**, 115101.
35. A. J. J. Bos, P. Dorenbos, A. Bessière, A. Lecointre, M. Bedu, M. Bettinelli and F. Piccinelli, *Radiation Measurements*, 2011, **46**, 1410-1416.
36. K. S. V. Nambi, V. N. Bapat and A. K. Ganguly, *Journal of Physics C-Solid State Physics*, 1974, **7**, 4403-4415.
37. H. Luo, A. J. J. Bos, A. Dobrowolska and P. Dorenbos, *Physical Chemistry Chemical Physics*, 2015, **17**, 15419-15427.
38. J. Kong, W. Zheng, Y. Liu, R. Li, E. Ma, H. Zhu and X. Chen, *Nanoscale*, 2015, **7**, 11048-11054.
39. C. W. Struck and W. H. Fonger, *Physical Review B*, 1971, **4**, 22-34.
40. W. I. Dobrov and R. A. Buchanan, *Applied Physics Letters*, 1972, **21**, 201-&.
41. P. W. Tasker and A. M. Stoneham, *Journal of Physics and Chemistry of Solids*, 1977, **38**, 1185-1189.

View Article Online
DOI: 10.1039/C7TC05221A

42. R. B. Murray and F. J. Keller, *Physical Review*, 1965, **137**, A942-A948.
43. N. F. Mott and A. M. Stoneham, *Journal of Physics C: Solid State Physics*, 1977, **10**, 3391.
44. F. Liu, Y. Liang, Y. Chen and Z. Pan, *Advanced Optical Materials*, 2016, **4**, 562-566.
45. Y. Liang, F. Liu, Y. Chen, X. Wang, K. Sun and Z. Pan, *Journal of Materials Chemistry C*, 2017, **5**, 6488-6492.